ACS OMEGA

http://pubs.acs.org/journal/acsodf

Article

Response Surface Method Based Modeling and Optimization of CMC-g Terpolymer Interpenetrating Network/Bentonite Superabsorbent Composite for Enhancing Water Retention

Shimaa Mohamed Elsaeed,* Elsayed Gamal Zaki, Ahmed Abdelhafes, and Ayman S. Al-Hussaini

Cite This: *ACS Omega* 2022, 7, 8219−8228

Read Online

ACCESS | Metrics & More | Article Recommendations | Supporting Information

ABSTRACT: Water shortages have become a serious issue, so the importance of developing innovative cellulose-based superabsorbent polymer (SAP) was experimentally assessed as an environmentally friendly alternative to acrylate-based SAPs for the optimization of water consumption. The development of a biodegradable superabsorbent hydrogel composite based on a graft copolymer of carboxymethyl cellulose (CMC) and mixtures of different comonomers such as an acrylamide-*co*-acrylic acid-*co*-2-acrylamido-2-methylpropanesulfonic acid (Am-*co*-AA-*co*-AMPS) CMC-*g*-TerPoly interpenetrating network was characterized by infrared spectroscopy (FT-IR), scan electron microscopy (SEM), atomic force microscope (AFM), thermal gravimetric analysis (TGA), and swelling capacity in different aqueous media. The optimized CMC-*g*-(TerPoly) composite showing outstanding superabsorbance with high water retention, the ratio of constituents, temperature, and pH effect on equilibrium swelling have been optimized by using multistage response surface methodology (RSM). In distilled water (d-water), the equilibrium water absorption capacity (EW) of the synthesized composite hydrogels (SAP-IPN1) is 1200 g (d-water/1g hydrogel) which is superior to any other commercial polyacrylate SAP hydrogels, while in saline water the EW is 650 g (s-water/1g hydrogel). The performance of the SAP-IPN for water retention was evaluated by studying several swelling/deswelling cycle measurements. The prepared SAP-IPN hydrogels were found to show pH and salt solution dependence on the swelling behavior. The new SAP-IPN can work with commercial SAP, which is recommended for application as a water reservoir in arid land for irrigation for agriculture purposes.

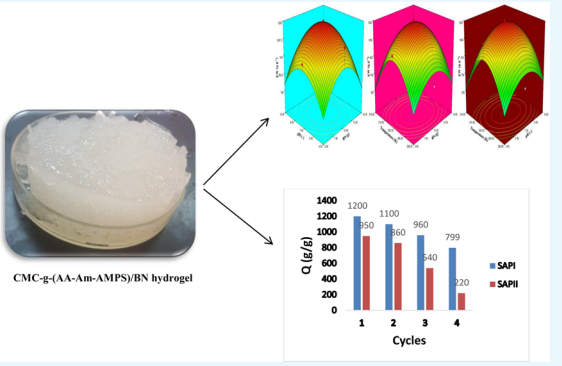

1. INTRODUCTION

The deficiency of water and desertification are serious problems in numerous regions of the world, and a serious problem is the concession of the development of agriculture. Egypt suffers from a deficiency of water, and we must find a tool to save water in order to save lives and to achieve sustainable development of agricultural goals. Recently, the production of eco-friendly, low cost, and biodegradable materials based on natural raw material alternating with petroleum synthetic sources that affect the environment has been studied.

Superabsorbent hydrogels were well-defined as three-dimensional networks of hydrophilic polymers fabricated by physical and/or chemical cross-linking. SAPs can absorb more than a thousand times their original weight, and they are able to retain and hold water or aqueous solution when compared with other normal absorbents even under difficult conditions,[1] which reduces the need for irrigation and consumption of water.

Use in agriculture,[2,3] wastewater treatment,[4−6] biosensors, drug release,[7] self-healing,[8] tissue engineering,[9] adsorbents for organic[10] and inorganic pollutants,[11,12] and enhanced oil recovery[13,14] are just a few of the applications for superabsorbent hydrogels. Generally, superabsorbent hydrogel based natural polymers such as chitosan,[15] cellulose,[16] starch,[17] collagen,[9] and sodium alginate[18] and their substitutes are more interesting because of their eco-friendliness, low cost, nontoxicity, biodegradability, and high hydrophilic network.[19] However, most of the SAPs existing on the market are mostly based on acrylate polymer from petroleum materials. The use of SAPs for agricultural applications has revealed encouraging results toward reduction of irrigation water consumption and improvement of water retention in soil.

Many research efforts have been concerned with the incorporation of inorganic clay for the preparation of superabsorbent hydrogel composites[2] such as kaolin,[3] bentonite, attapulgite,[4] montmorillonite (MMT),[5] and sodium silicate,[6] which enhance the swelling absorbance, thermal and mechanical stability, and other properties of SAP hydrogels and generate a

Received: June 18, 2021
Accepted: February 25, 2022
Published: March 4, 2022

https://doi.org/10.1021/acsomega.1c03194
ACS Omega 2022, 7, 8219−8228

new class of SAP for unique applications. Bentonite (BN)[7] is composed of aluminum silicate layered with exchangeable cations and −OH groups on the surface. BN has excellent absorption properties, which lead to improvement in the swelling and absorption of a water molecule into an SAP hydrogel.[8]

The objective of our work was to prepare an eco-friendly renewable superabsorbent based on a CMC-grafted-AA-*co*-AMPS-*co*-Am (CMC-*g*-TerPol) interpenetrating terpolymer network (IPN) hydrogel containing bentonite (BN) with better swelling, high water capacity, and reusability abilities that could compete with commercial SAPs for water storage and be used to save water and the environment. The swelling properties of the hydrogels in different solutions (water, NaCl) and different pH were thoroughly studied. The SAP-IPN hydrogels synthesized were characterized through infrared spectroscopy, scanning electron microscopy, atomic force spectroscopy, and thermal analysis of these hydrogel systems and evaluated. Water retention of prepared SAP-IPN hydrogels was evaluated.

2. EXPERIMENTAL SECTION

2.1. Materials. Carboxy methyl cellulose (CMC), acrylamide (AM), acrylic acid (AA), potassium persulfate (KPS), acrylamide-*co*-2-acrylamido-2-methylpropanesulfonic acid (AMPS), bentonite ($Al_2H_2Na_2O_{13}Si_4$)BN, *N*,*N*′ methylene bis(acrylamide) (MBA), NaOH, ethanol, and methanol were acquired from Sigma-Aldrich.

2.2. CMC-*g*-TerPols Superabsorbent Hydrogel Preparation. The CMC-*g*-TerPols superabsorbent hydrogel was synthesized using a free-radical polymerization process. A particular amount of d-water (100 mL) was required to dissolve 5 g of CMC. After that, an appropriate amount of bentonite BN (0, 5,10, 15 wt percent) was added, and the mixture was sonicated for 20 min to generate a homogeneous dispersed solution. AA, Am, and AMPS were consistently neutralized by adding NaOH with a concentration of 4 mol/L solution. KPS (0.8 g) in d-water was added to the mixture when the temperature reached 70 °C. MBA (0.06 g) in d-water was added to the entire mixture with a purge of N_2 after mixing for 15 min and lowering the temperature to 40 °C. To obtain CMC-*g*-(TerPols)/bentonite, (SAP-IPN1), the water bath was held at 70 °C to complete the polymerization reaction. To eliminate the unreacted monomers and other contaminants, this gel was broken into small pieces and washed with a sufficient ratio of distilled water and ethanol (60:40 mL). The SAP-IPN1 was produced and dried in a 60 °C oven overnight. As previously indicated, a comparable approach to make CMC-*g*-(TerPols) (SAP-IPN2) superabsorbent hydrogel without adding bentonite (BN) was needed. Equation 1 was used to obtain the grafting yield or percentage grafting (*G*):

$$G = (W_1 - W_0)/W_0 \times 100 \quad (1)$$

W_0 and W_1 represent the weights of pure CMC and grafting CMC-terpolymer, respectively. Table 1 shows the chemical composition of CMC superabsorbent hydrogels (1).

2.3. Characterization of SAP-IPN Hydrogels. The chemical structures were validated using Fourier transform infrared spectroscopy (ATI Matson Genesis Series FTIR). The thermal characteristics of the produced hydrogels were determined by thermogravimetric analysis of samples (TGA 55, Meslo, USA). Weight loss was plotted versus temperature after film samples were placed in a pan of platinum and heated in the range of 30−800 °C under N_2 atm at a heating rate of 10 °C per minute.

Table 1. Chemical Composition of CMC-g-(TerPol) Superabsorbent Hydrogel Composite

samples	CMC (g)	Ac (ml)	Am (g)	AMPS (g)	BN (%)	KPS (g)	MBA (g)
SAP-IPN1	5	2	2	2	5, 10, 15	0.8	0.06
SAP-IPN2	5	2	2	2	0	0.8	0.06

SEM was used to examine the morphology of the gel (which had been freeze-dried for 24 h) (SEM). Quanta FEG 250 scanning electron microscopes (FEI Company, USA) were used to capture surface images of hydrogels at the EDRC, DRC, and Cairo. SEM stubs were used to mount the samples. The SEM settings used were a 10.1 mm working distance and a 20 kV excitation voltage in the in-lens detector. AFM is the best-fitted instrument to identify the superficial structure of topography because it is capable of giving three-dimensional (3D) images. AFM is performed using a cantilever in static mode. Moreover, response surface methodology (RSM), an all graphic-based analysis, was carried out using the ANOVA software program.

2.4. Optimization Parameters by Response Surface Methodology (RSM). In addition to the individual effects of amounts of KPS, total monomers, MBA, and CMC on G (%), the simultaneous effects of these parameters on G (%) should be studied. However, the one-factor-at-a-time based study of these effects is very tedious, and thus, RSM, a statistical approach, has been adopted to optimize the synthesis parameters by performing the minimum number of experimental runs.

2.5. (CMC-TerPols) Superabsorbent Hydrogels Swelling and Equilibrium Water Absorbance Behavior. Dried SAP-IPN hydrogel (0.5 g) was immerged over d-water (200 mL) to reach the swelling equilibrium state (Q_{eq}) to assess equilibrium water absorbance and swelling of manufactured hydrogel. The solution was filtered out of the swelled gel, which was then dried. The swelled gel was then weighed, and eq 2 was used to calculate the equilibrium water absorbance

$$Q_{eq} = [(W_s - W_d)/W_d] \times 100 \quad (2)$$

where Q_{eq} is the equilibrium water absorption (g/g) or maximum water absorption capacity (EW) at time *t* (min), W_s is the swollen hydrogel weight (g), and W_d is the drying hydrogel weight (g).

In saline water (s-water), 0.9 wt % NaCl solution, and different buffer mediums, the swelling behavior of the CMC-g-(TerPols) superabsorbent was measured as follows: 100 mL of saline or buffer solution was put into 500 mL beakers containing 0.5 g of gel. After that, the swollen gels were filtered, and the swelling behavior of SAP-IPN was estimated using eq 2.

2.6. Water Retention Capacity of (CMC-TerPols) Superabsorbent Hydrogels. Water retention capacity (WRC) and water loss are the key features used to examine SAP-IPN hydrogels' ability to store water within their network structure.[9] It is very interesting to study the performance of the SAP-IPN hydrogels through deswelling and how the SAP-IPN hydrogels peform after some swelling/deswelling cycles. The water retention for porous SAP-IPN hydrogels prepared was measured by taking about 0.5 g of the dried SAP-IPN hydrogels and then adding in d-water until maximum swelling was reached.[10] Next, the swollen hydrogels were set into an oven at

https://doi.org/10.1021/acsomega.1c03194
ACS Omega 2022, 7, 8219−8228

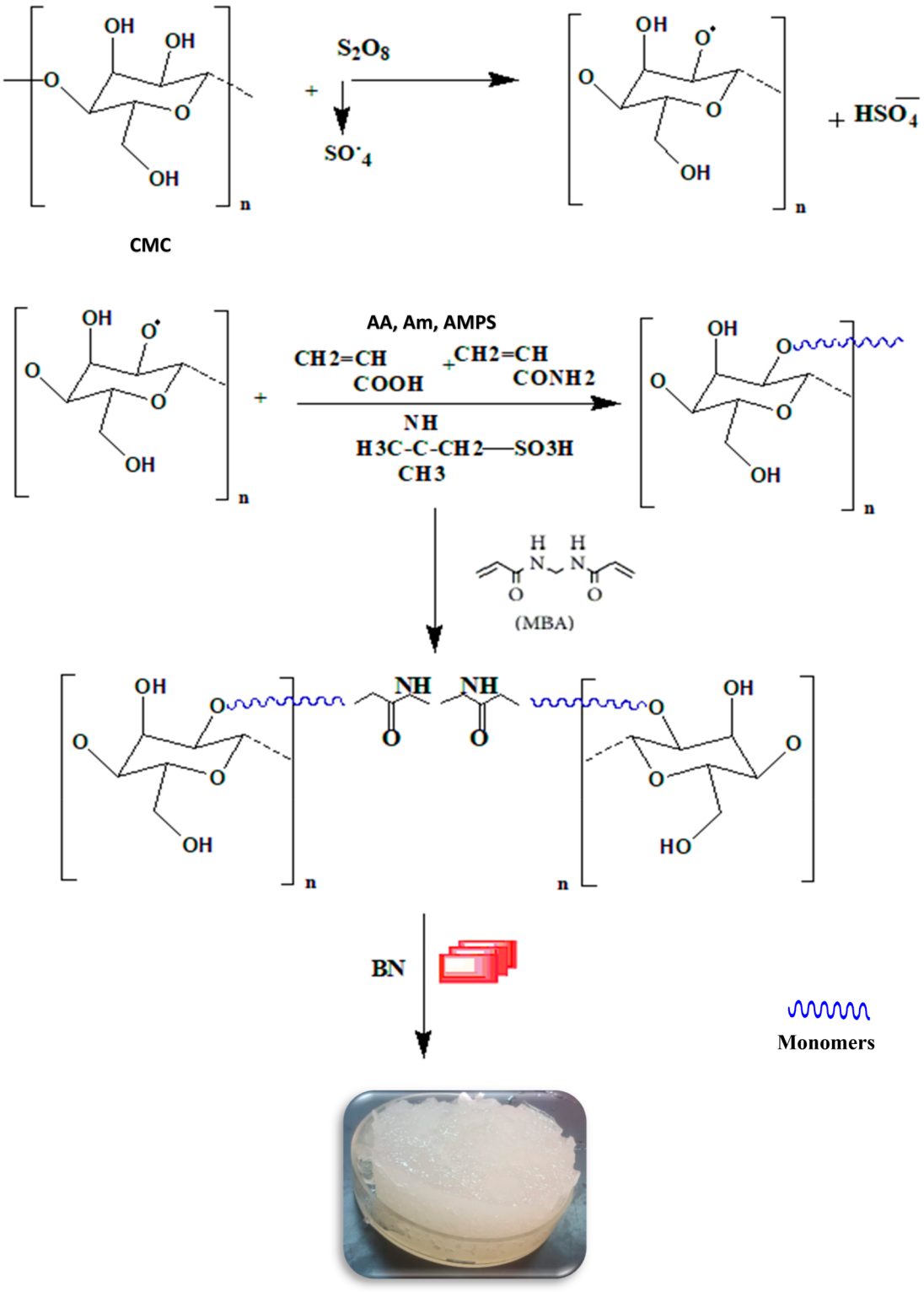

Figure 1. Scheme of synthesis of CMC-g-(TerPoly)/BN superabsorbent hydrogel. The photo was taken by Prof. Shimaa Elsaeed.

60 °C for different times. The water retention ratio (WR) of the prepared SAP-IPN hydrogels was calculated by eq 3[9]

$$\mathrm{WR}\,(\%) = (W_t/W_s) \times 100 \quad (3)$$

while W_t is the weight of the sample at a deswelling time (t) and W_s is the weight of the swollen sample.

3. RESULT AND DISCUSSION

3.1. Synthesis of CMC-g-TerPols and Spectral Analysis.

The expected process for graft polymerization and cross-linking of AA, AMPS, and Am onto CMC chains is shown in Figure 1. This development was carried out using APS as the radical initiator and MBA used as the cross-linking agent. Heating

https://doi.org/10.1021/acsomega.1c03194
ACS Omega 2022, 7, 8219−8228

causes APS to disintegrate at 70 °C under an N_2 purge to produce sulfate radicals, which grab hydrogen atoms from the CMC matrix's −OH groups to form macroradicals. In this stage, AA, Am, and AMPS monomers can be grafted onto these active macroradicals and MBA to form a three-dimensional interpenetrating network-IPN structure by cross-linking monomers with radicals on the CMC matrix. BN clay was distributed and bonded in a superabsorbent hydrogel network by forming a 3D-IPN network. By comparison, the FTIR spectra of CMC, BN, and SAP-IPN/BN, which found BN incorporation into the superabsorbent IPN, was confirmed.

Parts a−c of Figure 2 show the FTIR spectra of the CMC-g-(TerPolys)/BN superabsorbent composite, CMC, and BN clay,

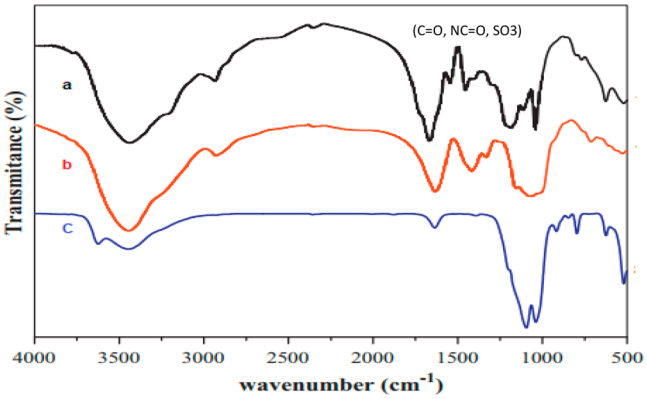

Figure 2. FTIR spectra of (a) CMC-g-(TerPoly)/BN hydrogel, (b) CMC, (c) BN.

respectively. The −OH stretching of CMC is related to the movement of the peak at 3437.7 cm^{-1}, and the band of CMC at 1000−1166 cm^{-1} is weakened due to the contribution of −OH of CMC in reaction. The peaks lose the −OH stretching of BN at 3400−3700 cm^{-1}, and the intensities of the peaks due to Si−O and Na−O of BN are weakened as revealed in Figure 2 at 860−920 cm^{-1}. The characteristic bands at 1548, 1670, and 1040 cm^{-1} are due to the carboxylate anion, carboxamide, and sulfonate group, respectively. Thus, SAP-IPN1 includes a cross-linked structure of CMC/BN with carrying carboxylate, carboxamide, and sulfonate groups in the network.[11]

3.2. Response Surface Methodology (RSM). *3.2.1. Optimization of the Synthesis Parameters.* The effects of amounts of KPS, total monomers, MBA, and CMC on the grafting ratio, G (%), and the simultaneous effects of these parameters on G (%) should be studied. RSM, a statistical approach, has been adopted to optimize the synthesis parameters. Face-centered central composite design (FCCCD), a standard RSM technique, was adopted to optimize the amounts of KPS (X_1, g), total monomers (X_2, g), MBA (X_3, g), and CMC (X_4, g) within 0.4−1.2, 3−9, 0.02−0.1, and 1−3 g, respectively (Table 1), to obtain the hydrogel presenting the maximum G (%) by using an empirical second-order polynomial (eq 4) to generate eq 5.

$$Y = \alpha_0 + \sum_{i=1}^{3} \alpha_i X_i + \sum_{i=1}^{3} \alpha_{ii} X_i^2 + \sum_{i=1}^{3} \sum_{j=1}^{2} \alpha_{ij} X_i X_j \quad (4)$$

$$G = -99.24 + 10.34X_1 + 69.14X_2 - 323.32X_3 - 18.86X_4 + 0.99X_1X_2 + 196.09X_1X_3 + 2.97X_1X_4 + 26.77X_2X_3 + 4.42X_2X_4 + 80.31X_3X_4 - 17.79{X_1}^2 - 6.67{X_2}^2 - 1778.51{X_3}^2 - 2.84{X_4}^2 \quad (5)$$

Here, Y, α_0, α_i, α_{ii}, and α_{ij} are predicted response, constant, linear, quadratic, and interaction coefficients, respectively. Moreover, the input variables, experimental, and software generated responses are given in Table 2. The acceptability of the quadratic model was confirmed from the sequential model sum of squares, model summary statistics tests, lack of fit tests, and ANOVA (Tables 3−6). The response surface plots presenting the interactive effects of X_1−X_2, X_1−X_3, X_1−X_4, X_2−X_3, X_2−X_4, and X_3−X_4 with G (%) are given in Figure 3a−f. Importantly, the optimum G (%) = 89.22% was obtained at 0.89, 6.01, 0.05, and 2 g for X_1, X_2, X_3, and X_4, respectively.

3.2.2. RSM Optimization on EW. The face-centered central composite design (FCCCD), a standard RSM technique, was adopted to optimize the individual and interactive effects of BN (X_5, g), pH (X_6, −), and temperature (X_7, K) on EW (g g^{-1}) by performing the minimum number of experimental runs. The input variables, i.e., X_5, X_6, and X_7, were varied within 5−15 g, 4−7, and 288−318 K, respectively (Table 7), for obtaining the maximum EW (g g^{-1}) by using the empirical second-order polynomial eq 4 to generate eq 6.

$$EW = -139454 + 180.89X_5 + 336.04X_6 + 915.56X_7 + 0.20X_5X_6 - 0.03X_5X_7 - 0.11X_6X_7 - 8.59{X_5}^2 - 21.11{X_6}^2 - 1.51{X_7}^2 \quad (6)$$

The input variables, software generated, and experimental responses are listed in Table 7. Here, the acceptability of quadratic model was confirmed from sequential model sum of squares, model summary statistics tests, lack of fit tests, and ANOVA (Table 8−11). The response surface plots envisaging interactive effects of X_5−X_6, X_5−X_7, and X_6−X_7 with EW (g g^{-1}) were given in Figure 4a−c. Importantly, the optimum EW of 1186.88 g g^{-1} was obtained at 10.10 g, 7.06, and 302.60 K for X_5, X_6, and X_7, respectively.

3.3. Analysis of Morphology. *3.3.1. SEM.* SEM is one of the most important aspects of superabsorbent hydrogels and can be used to examine the porosity and pore size of the hydrogel. SEM morphologies of the CMC-*g*-(AA-Am-AMPS)/BN, SAP-IPN1, and CMC-*g*-(AA-AMPS-Am), SAP-IPN2 were measured in the dry state. Parts a and b of Figure 5 show the SEM of the synthesized SAP hydrogel. It can be shown that for SAP-IPN1 (Figure 5a) the pores are smaller when they are connected to form a cross-linked network, which was beneficial for the diffusion of water into an SAP hydrogel and to the swelling rate. However, SAP-IPN2 Figure 5b), a porous structure with several big pores, which detached in a sheetlike manner, penetrate the water molecule but with a low rate of swelling. These SEM data showed that the BN was finely distributed throughout the composite, resulting in homogeneous composition.

3.3.2. AFM. An AFM image of SAP-IPN1 superabsorbent is shown in Figure 6b. AFM displays are in agreement with the SEM result that the CMC-grafted composite was rough and porous, which aided in the diffusion of water. The rougher the porous surface of the composite, the more water penetrates, resulting in more water absorbency by the composite. The root-mean-square (RMS) roughness of the composite is 191.2 nm,

https://doi.org/10.1021/acsomega.1c03194
ACS Omega 2022, 7, 8219−8228

Table 2. Design Matrix for Optimization of *G* (%)

	coded values				uncoded values				*G* (%)	
runs	X_1	X_2	X_3	X_4	KPS (g)	total monomers (g)	MBA (g)	CMC (g)	experimental	predicted
1	−1	−1	−1	−1	0.40	3.00	0.02	1.00	51.60	40.95
2	1	−1	−1	−1	1.20	3.00	0.02	1.00	35.60	34.35
3	−1	1	−1	−1	0.40	9.00	0.02	1.00	11.00	7.52
4	1	1	−1	−1	1.20	9.00	0.02	1.00	4.40	5.66
5	−1	−1	1	−1	0.40	3.00	0.10	1.00	5.00	17.14
6	1	−1	1	−1	1.20	3.00	0.10	1.00	34.00	23.08
7	−1	1	1	−1	0.40	9.00	0.10	1.00	10.00	−3.45
8	1	1	1	−1	1.20	9.00	0.10	1.00	6.00	7.25
9	−1	−1	−1	1	0.40	3.00	0.02	3.00	11.00	12.58
10	1	−1	−1	1	1.20	3.00	0.02	3.00	4.40	10.73
11	−1	1	−1	1	0.40	9.00	0.02	3.00	28.40	32.19
12	1	1	−1	1	1.20	9.00	0.02	3.00	44.40	35.09
13	−1	−1	1	1	0.40	3.00	0.10	3.00	10.00	1.62
14	1	−1	1	1	1.20	3.00	0.10	3.00	6.00	12.32
15	−1	1	1	1	0.40	9.00	0.10	3.00	30.00	34.08
16	1	1	1	1	1.20	9.00	0.10	3.00	46.00	49.53
17	−1	0	0	0	0.40	6.00	0.06	2.00	69.20	83.57
18	1	0	0	0	1.20	6.00	0.06	2.00	85.20	87.99
19	0	−1	0	0	0.80	3.00	0.06	2.00	22.80	27.63
20	0	1	0	0	0.80	9.00	0.06	2.00	17.20	29.52
21	0	0	−1	0	0.80	6.00	0.02	2.00	76.40	88.12
22	0	0	1	0	0.80	6.00	0.10	2.00	78.00	83.43
23	0	0	0	−1	0.80	6.00	0.06	1.00	57.20	82.29
24	**0**	**0**	**0**	**1**	**0.80**	**6.00**	**0.06**	**3.00**	**97.20**	**89.25**
25	**0**	**0**	**0**	**0**	**0.80**	**6.00**	**0.06**	**2.00**	**97.41**	**89.25**
26	**0**	**0**	**0**	**0**	**0.80**	**6.00**	**0.06**	**2.00**	**97.63**	**89.25**
27	**0**	**0**	**0**	**0**	**0.80**	**6.00**	**0.06**	**2.00**	**97.87**	**89.25**
28	**0**	**0**	**0**	**0**	**0.80**	**6.00**	**0.06**	**2.00**	**97.01**	**89.25**
29	**0**	**0**	**0**	**0**	**0.80**	**6.00**	**0.06**	**2.00**	**96.87**	**89.25**
30	**0**	**0**	**0**	**0**	**0.80**	**6.00**	**0.06**	**2.00**	**97.15**	**89.25**

Table 3. Sequential Model Sum of Squares

models	sum of squares	df[b]	mean square	*F*-value	*p*-value
mean vs total	67611.52	1	67611.52		
linear vs mean	420.70	4	105.18	0.0699	0.9905
2FI vs linear	3347.18	6	557.86	0.3093	0.9243
quadratic vs 2FI	**31718.01**	**4**	**7929.50**	**46.6224**	**< 0.0001**[a]
cubic vs quadratic	1403.84	8	175.48	1.0706	0.4707
residual	1147.35	7	163.91		
total	105648.60	30	3521.62		

[a]Significance. [b]Degrees of freedom.

Table 4. Model Summary Statistics

models	sd[a]	R^2	adj R^2	pred R^2	press
linear	38.79	0.0111	−0.1472	−0.3802	52499.90
2FI	42.47	0.0991	−0.3751	−1.9578	112507.27
quadratic	**13.04**	**0.9329**	**0.8703**	**0.6677**	**12641.55**
cubic	12.81	0.9698	0.8750	−2.9193	149077.96

[a]Standard deviation.

Table 5. Lack of Fit Tests

models	sum of squares	df[a]	mean square
linear	37616.38	20	1880.82
2FI	34269.20	14	2447.80
quadratic	**2551.19**	**10**	**255.12**
cubic	1147.35	2	573.67
pure error	0.00	5	0.00

[a]Degrees of freedom.

and the average roughness (Sa) is 141.0 nm. Figure 6a shows that th eRMS of SAP-IPN2 is 170.1 nm, and Sa is 111.2 nm, which means lower water absorbance than SAP-IPN1. This result agrees with SEM and the swelling rate behavior.[12]

3.4. Thermogravimetric (TGA) Analysis. The effect of grafting and cross-linking of monomers chains onto CMC and interpenetration of bentonite within the CMC on the thermodynamic stability was investigated. The thermal property of the SAP-IPN1 and SAP-IPN2 hydrogels was evaluated by comparing the weight loss (%) in the temperature range of 100−600 °C as shown in Figure S1. Three-stage decomposition mechanism was found, and maximum weight loss was observed after the first stage decomposition of cross-linked samples; this indicates the chemical modification of CMC. Table S1 summarizes the weight loss of two hydrogels; in every case the hydrogel's initial decomposition temperature (IDT) was 200−300 °C, which is due to the loss of moisture or volatile compounds. The second stage was observed in the temperature range of 400−500 °C due to the elimination of side chains. Finally, the third stage of decomposition was observed at 600 °C due to the breakdown of the cross-linked structure. In comparison, the rate of decomposition was lower in case of

https://doi.org/10.1021/acsomega.1c03194
ACS Omega 2022, 7, 8219−8228

Table 6. ANOVA

source	sum of squares	df[b]	mean square	F-value	p-value
model	**35485.89**	**14**	**2534.71**	**14.90**	**< 0.0001**[a]
X_1	88.00	1	88.00	0.52	0.4830
X_2	16.06	1	16.06	0.09	0.7629
X_3	98.94	1	98.94	0.58	0.4575
X_4	217.71	1	217.71	1.28	0.2757
X_1X_2	22.56	1	22.56	0.13	0.7208
X_1X_3	157.50	1	157.50	0.93	0.3511
X_1X_4	22.56	1	22.56	0.13	0.7208
X_2X_3	165.12	1	165.12	0.97	0.3401
X_2X_4	**2814.30**	**1**	**2814.30**	**16.55**	**0.0010**[a]
X_3X_4	165.12	1	165.12	0.97	0.3401
X_1^2	20.98	1	20.98	0.12	0.7303
X_2^2	**9341.46**	**1**	**9341.46**	**54.92**	**<0.0001**[a]
X_3^2	20.98	1	20.98	0.12	0.7303
X_4^2	20.98	1	20.98	0.12	0.7303
residual	2551.19	15	170.08	**std dev**	13.04
lack of fit	2551.19	10	255.12	**mean**	47.47
pure error	0	5	0.00	**CV (%)**	27.47
cor total	38037.08	29		**press**	12641.55

[a]Degrees of freedom. [b]Significance.

Table 7. Design Matrix for Optimization of ESR (g g^{-1})

	coded values			uncoded values			ESR (g g^{-1})	
runs	X_5	X_6	X_7	BN (g)	pH (−)	T (K)	experimental	predicted
1	−1	−1	−1	5	4	288	910	425.53
2	1	−1	−1	15	4	288	870	440.49
3	−1	1	−1	5	10	288	800	471.49
4	1	1	−1	15	10	288	760	498.36
5	−1	−1	1	5	4	318	930	404.63
6	1	−1	1	15	4	318	830	411.03
7	−1	1	1	5	10	318	910	429.43
8	1	1	1	15	10	318	820	447.73
9	−1	−1	−1	5	7	303	1000	962.71
10	1	−1	−1	15	7	303	900	979.33
11	−1	1	−1	10	4	303	1100	975.35
12	1	1	−1	10	10	303	850	1016.69
13	−1	−1	1	10	7	288	750	863.90
14	1	−1	1	10	7	318	900	828.14
15	**−1**	**1**	**1**	**10**	**7**	**303**	**1200**	**1185.99**
16	**1**	**1**	**1**	**10**	**7**	**303**	**1198**	**1185.99**
17	**−1**	**0**	**0**	**10**	**7**	**303**	**1191**	**1185.99**
18	**1**	**0**	**0**	**10**	**7**	**303**	**1196**	**1185.99**
19	**0**	**−1**	**0**	**10**	**7**	**303**	**1200**	**1185.99**
20	**0**	**1**	**0**	**10**	**7**	**303**	**1197**	**1185.99**

SAP-IPN2 than SAP-IPN1; this implies a more compact and stable cross-linked polymeric network which may be because the incorporation of bentonite into the polymeric network provides a protective barrier to both mass and energy transport in hydrogel composites interpenetrating network.

3.5. Measurement of Equilibrium Water Absorbency and Swelling Behavior of SAP-IPN. *3.5.1. Effect of BN on Water Absorption Capacity.* The incorporation of BN clay into SAP-IPN hydrogels shows an effect on ES. The highest ES value was found to be at 10% BN. It is shown in Table S2 that SAP-IPN1 is about 1200 g/g. In contrast, in SAP-IPN2 it is 950 g/g. This may be due to the presence of −OH groups on the surface of BN interacting with hydroxyl, carboxylate, carboxamide, and sulfonate groups in the network, which increases and enhances the affinity of the network structure to water molecule.[13]

As a result, as clay concentration rises, it may act as an extra cross-linking point in polymer networks, increasing the cross-

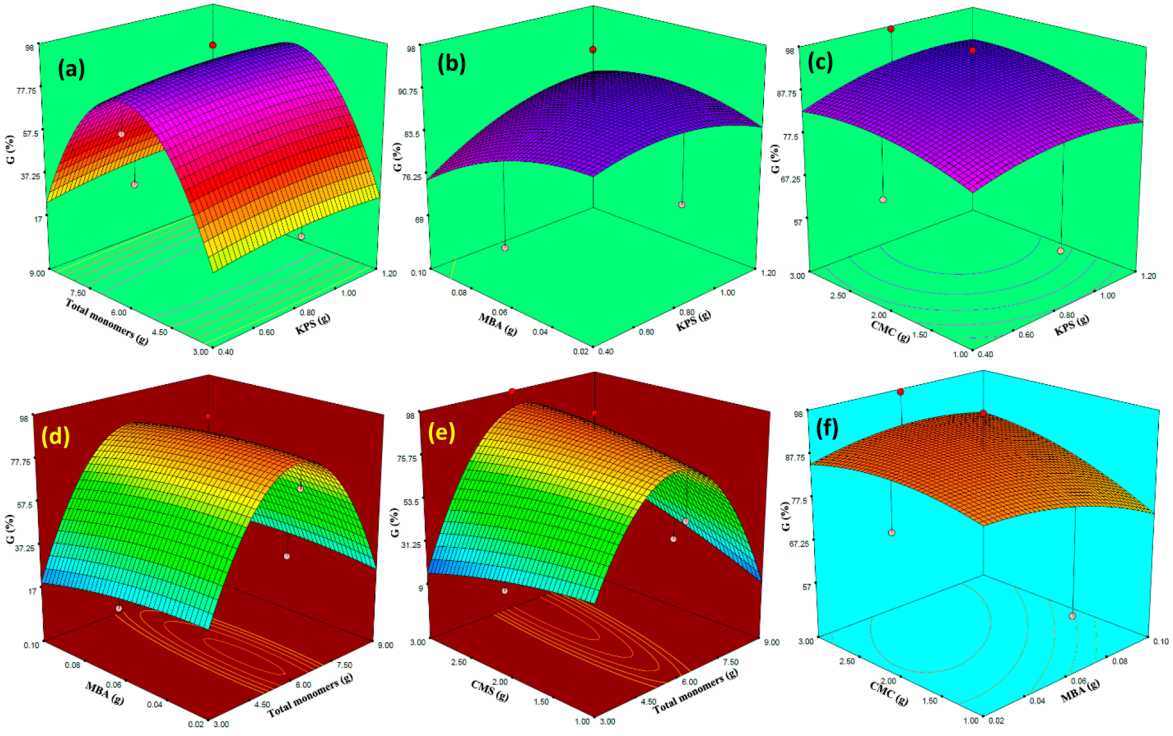

Figure 3. 3D response surface plots of G (%) vs (a) total monomers (g)/KPS (g), (b) MBA (g)/KPS (g), (c) CMC (g)/KPS (g), (d) MBA (g)/total monomers (g), (e) CMC (g)/total monomers (g), and (f) CMC (g)/MBA (g).

https://doi.org/10.1021/acsomega.1c03194
ACS Omega 2022, 7, 8219−8228

Table 8. Sequential Model Sum of Squares

models	sum of squares	df[b]	mean square	*F*-value	*p*-value
mean vs total	1.32×10^7	1	1.32×10^7		
linear vs mean	8159.83	3	2719.94	0.02	0.9959
2FI vs linear	331.53	3	110.51	6.69×10^{-4}	1.0000
quadratic vs 2FI	**2.06×10^6**	**3**	**6.87×10^5**	**78.79**	**< 0.0001[a]**
cubic vs quadratic	83116.43	4	20779.11	30.78	0.0004
residual	4050.27	6	675.05		
total	1.54×10^7	20	7.70×10^5		

[a]Significance. [b]Degrees of freedom.

Table 9. Model Summary Statistics

models	sd[a]	R^2	adj R^2	pred R^2	press
linear	366.39	0.0038	−0.1830	−0.7635	3.80×10^6
2FI	406.44	0.0039	−0.4558	−6.2782	1.57×10^7
quadratic	**93.36**	**0.9596**	**0.9232**	**0.6929**	**6.62×10^5**
cubic	25.98	0.9981	0.9941	−1.3082	4.98×10^6

[a]Standard deviation.

Table 10. Lack of Fit Tests

models	sum of squares	df[a]	mean square
linear	2.15×10^6	11	1.95×10^5
2FI	2.15×10^6	8	2.68×10^5
quadratic	**87166.70**	**5**	**17433.34**
cubic	4050.27	1	4050.27
pure error	0.00	5	0.00

[a]Degrees of freedom.

Table 11. ANOVA

source	sum of squares	df[a]	mean square	*F*-value	*p*-value
model	**2068865.10**	**9**	**229873.90**	**26.37**	**<0.0001[b]**
X_5	691.23	1	691.23	0.08	0.7840
X_6	4271.66	1	4271.66	0.49	0.4999
X_7	3196.94	1	3196.94	0.37	0.5583
X_5X_6	**70.81**	**1**	**70.81**	**0.17**	**0.0930**
X_5X_7	36.64	1	36.64	0.01	0.9496
X_6X_7	224.08	1	224.08	0.03	0.8758
X_5^2	**127078.98**	**1**	**127078.98**	**14.58**	**0.0034**
X_6^2	**99239.85**	**1**	**99239.85**	**11.39**	**0.0071**
X_7^2	**317837.10**	**1**	**317837.10**	**36.46**	**0.0001**
residual	87166.70	10	8716.67	**std. dev.**	
lack of fit	87166.70	5	17433.34	**mean**	
pure error	0.00	5	0.00	**CV (%)**	
cor total	2156031.80	19		**press**	

[a]Degrees of freedom. [b]Significance.

linking density and thus decreasing the network spaces for water storage.

3.5.2. Water Absorption Capacity in Saline Water. The water absorbance of both SAP-IPN hydrogels was measured in s-water 0.9 wt % NaCl solution and d-water. Figure S2a,b depicts a decrease in swelling behavior when compared to the data in d-water. Ionic hydrogels have a charge screening effect, which produces a nonperfect anion−anion repulsion, which results in a decreased ionic pressure between the SAP hydrogels and water molecules, resulting in a decrease in water absorption capacity. d-Water displays good results as it has lower ionic concentration, which aids in better water intake by osmotic pressure.

3.5.3. Swelling Behavior in Various Buffer Media. Table S3 reveals the equilibrium swelling (EW) of both SAP-IPN hydrogels at different pH values (the pH values are adjusted by using a pH-meter AD1030 Professional pH-ORP-Temp Bench Meter ADWA). In acidic media, both SAP-IPN hydrogels had a low EW and a maximum value in neutral media. The increase in pH causes carboxyl groups in the CMC to be changed to carboxylate ions, causing repulsion and the formation of space between chains, allowing water particles to enter the SAP-IPN hydrogels and increasing water absorption. However, as the pH rises over pH 7, the ability for absorption decreases. This could be due to the presence of Na^+ cations in basic solutions, which prevent anion−anion repulsion and decrease spaces between chains, thereby decreasing water absorption capacity.[14,15] Table S3 summarizes the values of EW in different media.

3.5.4. Water Retention Capability of SAP-IPN hydrogels. To study the water absorbency capability to estimate the reusability of the SAP, the SAP-IPN hydrogels were put in d-water to reach the maximum swelling ratio. The were dried at a temperature of 30 °C several times. The swelling and deswelling cycles of the SAP-IPN1 and SAP-IPN2 were repeated four times. As shown in Figure S3, the equilibrium swelling capacity of SAP-IPN2 decreased from 950 to 220 g/g after four sequential swelling/deswelling cycles. In contrast, the equilibrium swelling capacity of SAP-IPN1 was 1200 g/g in the first swelling/deswelling cycle and 799.11 g/g in the fourth swelling/deswelling cycle, respectively. The slight loss of swelling capacity for SAP-IPN1 is due to the stable 3D-network, and the incorporation of rigid BN-clay prevented linking of grafted polymeric chains and weakened the hydrogen-bonding interaction between COOH groups. This decreased the degree of physical cross-linking and improved water absorption. Therefore, this structure of the SAP-IPN1 hydrogel network avoids the collapse during the swelling/deswelling cycles, which makes reduced damage of swelling capacity and enable to resist high temperature.[16] As a result, the SAP-IPN/BN composite has the ability to retain and hold water more than four cycles with the same efficiency. In addition, SAP-IPN/BN could be used as a water storage source in the arid region and desert land[17] for agriculture application.[18]

3.6. Comparison of the Results. Several biopolymer-based superabsorbent hydrogels, gums, oxide/co/biopolymers, and IPN hydrogels for water retention of varying components, temperatures, and effect of pH values have been provided (Table S4). In this work, it is important to note that the addition of bentonite to CMC increases the structure of hydrogel and, therefore, allows networks to absorb more water. From Table S4, it could be observed that the terpolymer interpenetrating network/bentonite of CMC was either closer to or much better than previously reported super absorbent hydrogels within the specified working range.

https://doi.org/10.1021/acsomega.1c03194
ACS Omega 2022, 7, 8219−8228

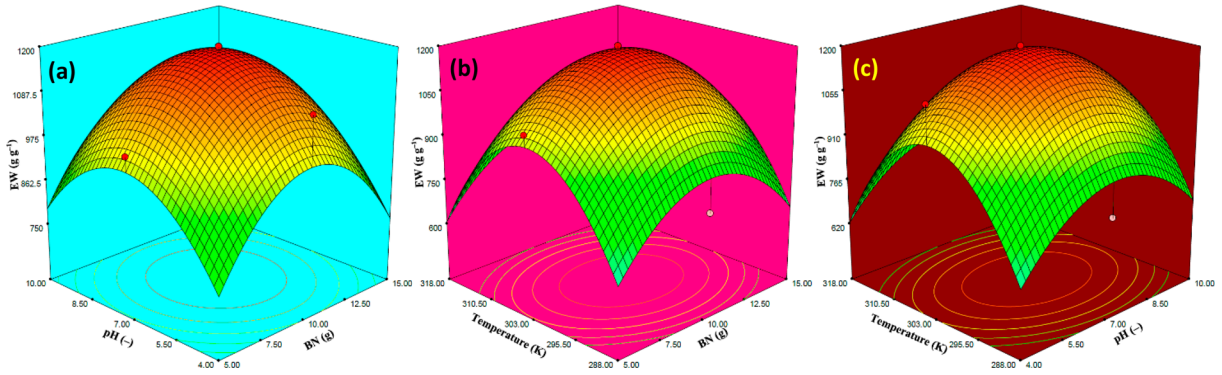

Figure 4. 3D response surface plots of EW (g g^{-1}) vs (a) pH (−)/BN (g), (b) temperature (K)/BN (g), and (c) temperature (K)/pH (−).

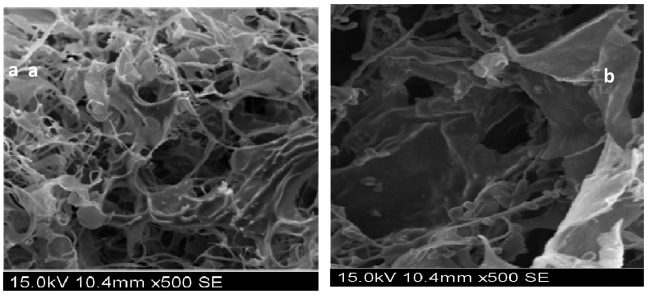

Figure 5. SEM morphology of (a) SAP-IPN1, (b) SAP-IPN2.

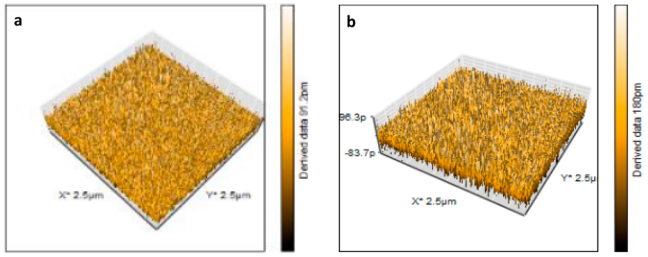

Figure 6. AFM of (a) SAP-IPN2, (b) SAP-IPN1.

Hydrogels can be used in real life as soil conditioners, and now there are prototypes and real samples send to farmers for use in soil. These trial are underway.

3.7. Mechanism of Swelling Behavior of the SAP Hydrogel. The promising property of hydrogels is the capability to swell when interacting with an aqueous solution (Figure S4). The water molecules penetrate the polymeric network. Frequently, the meshes of the 3D network structure in the rubbery stage will start expanding, allowing more penetration of aqueous molecules within the hydrogel 3D structure network. The rate of swelling is a very important feature of hydrogel swelling behavior.[19] It is measured by numerous physico-chemical issues such as the particle size, porosity, and the types of porous structure such as nonporous, micro-, macro-, and superporous (SAP).[20−22] Superabsorbent hydrogels (SAP) are connected to form the open canal and act as a tube system for fast uptake of water into the porous structure until an equilibrium state is reached. The fast swelling of SAP hydrogel is attributed to the absorption of water through a capillary force rather than by normal absorption.[23,24] Conventional SAP hydrogels are characterized by fast swelling, high swelling ratio, and weak mechanical properties. To overcome their weak mechanical properties, a superabsorbent hydrogel/composite has been prepared to improve mechanical properties.[25] Osmotic pressure, electrostatic, and viscoelastic forces are the three focal forces controlling the swelling behavior of hydrogels. The different models describe and study the effect of these forces on swelling behavior. Achilleos et al. have developed a system for the actual time of dynamic distortion through swelling processes.[26] The swelling is not a repeated process. When compared to the osmotic force, there is an opposite elasticity force, which balances the expanding of the network and avoids shrinking. At the equilibrium state, there is no additional swelling due to elasticity, and osmotic forces are equal.

4. CONCLUSIONS

An innovative CMC-*g*-(TerPolymer) interpenetrating superabsorbent network (SAP-IPN) was evaluated as an eco-friendly alternate to acrylate-based SAPs for the optimization of water consumption.

The main findings are summarized in the following points:

- CMC-*g*-TerPols superabsorbent hydrogels were prepared successfully by a free-radical polymerization technique using acrylic acid, acrylamide, and AMPS and cross-linked using MBA. The proposed mechanism for the grafting was a free-radical mechanism using potassium persulfate as the initiator.
- A composite (SAP-IPN1 and SAP-IPN2) based on the newly synthesized hydrogel was also prepared by incorporating bentonite in the polymer matrix.
- The newly synthesized hydrogels were characterized by FTIR. They confirm the successful grafting and incorporation of the bentonite within the polymeric matrix.
- The thermal stability of SAP-IPN1 and SAP-IPN2 was investigated by TGA, a more condensed and stable cross-linked polymeric network in SAP-IPN1 that may be due to the incorporation of bentonite into the polymeric network to provide a protective barrier for both mass and energy transport.
- The equilibrium swelling properties is optimized by RSM (response surface methodology).
- The incorporation of BN clay into SAP-IPN hydrogels empowers effects on EW.
- AFM displays in agreement with the SEM result that the CMC-grafted composite was a rough and porous structure.
- The newly developed SAP hydrogel composite may be able to compete with synthetic SAP hydrogels on the market today and are promising for agricultural

https://doi.org/10.1021/acsomega.1c03194
ACS Omega 2022, 7, 8219−8228

applications for saving water in the irrigation of arid and desert land and other novel applications

■ ASSOCIATED CONTENT

Supporting Information

The Supporting Information is available free of charge at https://pubs.acs.org/doi/10.1021/acsomega.1c03194.

TGA Analysis of CMC-g-(TerPolys) superabsorbent hydrogel, swelling ratio of SAP-IPN as function of time, water retention capacity of SAP-IPN, effect of BN concentration on water absorption capacity, swelling behavior in various buffer media, and comparative study (PDF)

■ AUTHOR INFORMATION

Corresponding Author

Shimaa Mohamed Elsaeed − *Egyptian Petroleum Research Institute, Nasr City, Cairo 11727, Egypt; National Committee of Women in Science (NCWS), ASRT, Cairo 11334, Egypt;* orcid.org/0000-0002-8373-3319; Email: shy_saeed@yahoo.com

Authors

Elsayed Gamal Zaki − *Egyptian Petroleum Research Institute, Nasr City, Cairo 11727, Egypt;* orcid.org/0000-0001-7053-3169

Ahmed Abdelhafes − *Chemistry Department, Faculty of Science, Port Said University, Port Said 42521, Egypt*

Ayman S. Al-Hussaini − *Chemistry Department, Faculty of Science, Port Said University, Port Said 42521, Egypt;* orcid.org/0000-0002-6212-3706

Complete contact information is available at: https://pubs.acs.org/10.1021/acsomega.1c03194

Author Contributions

The manuscript was written through contributions of all authors. All authors have given approval to the final version.

Notes

The authors declare no competing financial interest.

■ ACKNOWLEDGMENTS

The authors acknowledge the Egyptian Petroleum Research Institute (EPRI) and Port-Said University for supporting this work. The authors acknowledge and appreciate Dr. Nayan Ranjan, Assistance Professor, Abul Kalam Azad University of Technology, India, for supporting this work. The authors greatly acknowledge funding by the Science and Technology Development Fund (STDF) (Capacity Building Project ID: 38280), Cairo, Egypt.

■ ABBREVIATIONS

CMC, carboxy methyl cellulose; Am, acrylamide; AA, acrylic acid; AMPS, 2-acrylamido-2-methylpropane sulfonic acid; MBA, *N,N′*-methylene bisacrylamide; KPS, pot persulfate; SAP, superabsorbent polymer; BN, bentonite; IPN, interpenetrating network; FTIR, Fourier-transform infrared spectroscopy; TGA, thermal gravimetric analysis; SEM, scan electron microscope; AFM, atomic force microscope; RSM, response surface methodology; EW, equilibrium water absorption capacity or equilibrium swelling,

■ REFERENCES

(1) Alam, M. N.; Islam, M. S.; Christopher, L. P. Sustainable Production of Cellulose-Based Hydrogels with Superb Absorbing Potential in Physiological Saline. *ACS omega* **2019**, *4* (5), 9419−9426.

(2) El Salmawi, K. M.; Ibrahim, S. M. Characterization of Superabsorbent Carboxymethylcellulose/Clay Hydrogel Prepared by Electron Beam Irradiation. *Macromol. Res.* **2011**, *19* (10), 1029.

(3) Zaharia, A.; Sarbu, A.; Radu, A.-L.; Jankova, K.; Daugaard, A.; Hvilsted, S.; Perrin, F.-X.; Teodorescu, M.; Munteanu, C.; Fruth-Oprisan, V. Preparation and Characterization of Polyacrylamide-Modified Kaolinite Containing Poly [Acrylic Acid-Co-Methylene Bisacrylamide] Nanocomposite Hydrogels. *Appl. Clay Sci.* **2015**, *103*, 46−54.

(4) Liu, P.; Jiang, L.; Zhu, L.; Guo, J.; Wang, A. Synthesis of Covalently Crosslinked Attapulgite/Poly (Acrylic Acid-Co-Acrylamide) Nanocomposite Hydrogels and Their Evaluation as Adsorbent for Heavy Metal Ions. *J. Ind. Eng. Chem.* **2015**, *23*, 188−193.

(5) Irani, M.; Ismail, H.; Ahmad, Z. Preparation and Properties of Linear Low-Density Polyethylene-g-Poly (Acrylic Acid)/Organo-Montmorillonite Superabsorbent Hydrogel Composites. *Polym. Test.* **2013**, *32* (3), 502−512.

(6) Lu, Y.; Chang, P. R.; Zheng, P.; Ma, X. Porous 3D Network Rectorite/Chitosan Gels: Preparation and Adsorption Properties. *Appl. Clay Sci.* **2015**, *107*, 21−27.

(7) Zhang, H.; Omer, A. M.; Hu, Z.; Yang, L.-Y.; Ji, C.; Ouyang, X. Fabrication of Magnetic Bentonite/Carboxymethyl Chitosan/Sodium Alginate Hydrogel Beads for Cu (II) Adsorption. *Int. J. Biol. Macromol.* **2019**, *135*, 490−500.

(8) Hao, Q.; Chen, T.; Wang, R.; Feng, J.; Chen, D.; Yao, W. A Separation-Free Polyacrylamide/Bentonite/Graphitic Carbon Nitride Hydrogel with Excellent Performance in Water Treatment. *J. Clean. Prod.* **2018**, *197*, 1222−1230.

(9) Sharma, K.; Kaith, B. S.; Kumar, V.; Kalia, S.; Kumar, V.; Swart, H. C. Water Retention and Dye Adsorption Behavior of Gg-Cl-Poly (Acrylic Acid-Aniline) Based Conductive Hydrogels. *Geoderma* **2014**, *232*, 45−55.

(10) Chen, Y.-C.; Chen, Y.-H. Thermo and PH-Responsive Methylcellulose and Hydroxypropyl Methylcellulose Hydrogels Containing K2SO4 for Water Retention and a Controlled-Release Water-Soluble Fertilizer. *Sci. Total Environ.* **2019**, *655*, 958−967.

(11) Casaburi, A.; Rojo, Ú. M.; Cerrutti, P.; Vázquez, A.; Foresti, M. L. Carboxymethyl Cellulose with Tailored Degree of Substitution Obtained from Bacterial Cellulose. *Food Hydrocoll.* **2018**, *75*, 147−156.

(12) Pal, K.; Banthia, A. K.; Majumdar, D. K. Polymeric Hydrogels: Characterization and Biomedical Applications. *Des. monomers Polym.* **2009**, *12* (3), 197−220.

(13) Witono, J. R.; Noordergraaf, Iw.; Heeres, H. J.; Janssen, L. Water Absorption, Retention and the Swelling Characteristics of Cassava Starch Grafted with Polyacrylic Acid. *Carbohydr. Polym.* **2014**, *103*, 325−332.

(14) Priyadarshi, R.; Kumar, B.; Rhim, J.-W. Green and Facile Synthesis of Carboxymethylcellulose/ZnO Nanocomposite Hydrogels Crosslinked with Zn2+ Ions. *Int. J. Biol. Macromol.* **2020**, *162*, 229−235.

(15) Wang, W.; Wang, Q.; Wang, A. PH-Responsive Carboxymethylcellulose-g-Poly (Sodium Acrylate)/Polyvinylpyrrolidone Semi-IPN Hydrogels with Enhanced Responsive and Swelling Properties. *Macromol. Res.* **2011**, *19* (1), 57−65.

(16) Li, S.-X.; Wang, Z.-H.; Malhi, S. S.; Li, S.-Q.; Gao, Y.-J.; Tian, X.-H. Nutrient and Water Management Effects on Crop Production, and Nutrient and Water Use Efficiency in Dryland Areas of China. *Adv. Agron.* **2009**, *102*, 223−265.

(17) Cheng, D.; Liu, Y.; Yang, G.; Zhang, A. Water-and Fertilizer-Integrated Hydrogel Derived from the Polymerization of Acrylic Acid and Urea as a Slow-Release N Fertilizer and Water Retention in Agriculture. *J. Agric. Food Chem.* **2018**, *66* (23), 5762−5769.

(18) Wei, J.; Yang, H.; Cao, H.; Tan, T. Using Polyaspartic Acid Hydro-Gel as Water Retaining Agent and Its Effect on Plants under Drought Stress. *Saudi J. Biol. Sci.* **2016**, *23* (5), 654−659.

(19) Chen, J.; Park, H.; Park, K. Synthesis of Superporous Hydrogels: Hydrogels with Fast Swelling and Superabsorbent Properties. *J. Biomed. Mater. Res. An Off. J. Soc. Biomater. Japanese Soc. Biomater. Aust. Soc. Biomater.* **1999**, *44* (1), 53−62.
(20) Qi, X.; Zeng, Q.; Tong, X.; Su, T.; Xie, L.; Yuan, K.; Xu, J.; Shen, J. Polydopamine/Montmorillonite-Embedded Pullulan Hydrogels as Efficient Adsorbents for Removing Crystal Violet. *J. Hazard. Mater.* **2021**, *402*, 123359.
(21) Zeng, Q.; Qi, X.; Zhang, M.; Tong, X.; Jiang, N.; Pan, W.; Xiong, W.; Li, Y.; Xu, J.; Shen, J. Efficient Decontamination of Heavy Metals from Aqueous Solution Using Pullulan/Polydopamine Hydrogels. *Int. J. Biol. Macromol.* **2020**, *145*, 1049−1058.
(22) Qi, X.; Wei, W.; Li, J.; Zuo, G.; Hu, X.; Zhang, J.; Dong, W. Development of Novel Hydrogels Based on Salecan and Poly (N-Isopropylacrylamide-Co-Methacrylic Acid) for Controlled Doxorubicin Release. *RSC Adv.* **2016**, *6* (74), 69869−69881.
(23) Dorkoosh, F. A.; Verhoef, J. C.; Borchard, G.; Rafiee-Tehrani, M.; Verheijden, J. H. M.; Junginger, H. E. Intestinal Absorption of Human Insulin in Pigs Using Delivery Systems Based on Superporous Hydrogel Polymers. *Int. J. Pharm.* **2002**, *247* (1−2), 47−55.
(24) Kim, D.; Park, K. Swelling and Mechanical Properties of Superporous Hydrogels of Poly (Acrylamide-Co-Acrylic Acid)/Polyethylenimine Interpenetrating Polymer Networks. *Polymer (Guildf).* **2004**, *45* (1), 189−196.
(25) Omidian, H.; Rocca, J. G.; Park, K. Advances in Superporous Hydrogels. *J. Control. release* **2005**, *102* (1), 3−12.
(26) Achilleos, E. C.; Prud'Homme, R. K.; Christodoulou, K. N.; Gee, K. R.; Kevrekidis, I. G. Dynamic Deformation Visualization in Swelling of Polymer Gels. *Chem. Eng. Sci.* **2000**, *55* (17), 3335−3340.

https://doi.org/10.1021/acsomega.1c03194
ACS Omega 2022, 7, 8219−8228